THE JOURNAL OF PHYSICAL CHEMISTRY C

Article

pubs.acs.org/JPCC

Modeling the Self-Assembly of Organic Molecules in 2D Molecular Layers with Different Structures

Joost van der Lit,[†] Jolien L. Marsman,[†] Rik S. Koster, Peter H. Jacobse, Stephan A. den Hartog, Daniel Vanmaekelbergh, Robertus J. M. Klein Gebbink, Laura Filion,* and Ingmar Swart*

Debye Institute for Nanomaterials Science, Utrecht University, PO Box 80000, 3508 TA Utrecht, The Netherlands

Supporting Information

ABSTRACT: If organic molecules are to be used as the active component in devices, self-assembly represents the most attractive route to control the geometric structure and therefore part of the device performance. High-resolution scanning tunneling microscopy measurement combined with density functional theory and Monte Carlo calculations are used to study the stability of self-assemblies of molecules with bonding motifs spanning (nearly) the entire range of intermolecular interaction strengths. Our atomistic model reproduces the experimentally observed crystal structures with sub-Ångström precision in all cases. In addition, it is able to identify metastable structures through thermodynamic analysis.

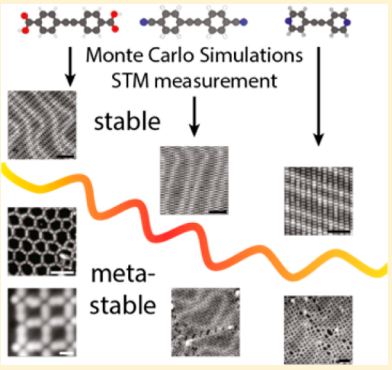

INTRODUCTION

The ability to control the properties of surfaces is of key importance for many technologies. One attractive route to achieve this is via the adsorption of organic molecules.[1] In particular, molecular layers can impart potentially useful features to surfaces, such as resistance to corrosion, templating, and biocompatibility.[2,3] Ordered molecular architectures can give rise to more sophisticated functionalities such as gas sensing,[4] molecular machines,[5] and molecular circuitry for electronics.[6,7] Both the types of molecules as well as the geometric structure of the final self-assembled layer influence the properties of the material. Hence, structural control is of great importance.

On a surface, the interplay of molecule−molecule and molecule−substrate interactions governs the geometry of the final layer. For example, molecules with different functional groups but the same chemical backbone give rise to different self-assembled structures (*vide infra*).[8] In addition, the same molecule can form multiple structures,[9] either because multiple crystals are stable or because a local minimum in free energy is kinetically favored. Specifically, phenomena such as kinetic trapping and pathway complexity can result in the formation of metastable structures, i.e., structures corresponding to local minima in the free energy landscape.[10] Such phases are well-known experimentally, and a significant research effort is devoted to circumvent their formation.[11−13] On the other hand, *control* over metastable structures offers an additional avenue to tune the final geometry of the self-assembled phase via experimental parameters, e.g., the cooling rate.[14]

Considering the vast parameter space and the importance of the structure for the final properties, a method that predicts which structures are thermodynamically stable and which are metastable based on just the chemical composition of the constituent molecules and the substrate used is therefore highly desirable. Thus, far, extracting thermodynamic information from models of molecular self-assembly has received little attention.

Different types of models have been used to simulate self-assembly. This includes models in which molecules are represented as geometric shapes that move on a lattice.[9,15−17] The interactions between these shapes are typically described using a set of binding rules extracted from density functional theory (DFT). Alternatively, atomistic models have been devised.[18,19] In the absence of chemical reactions, intermolecular interactions are dominated by van der Waals attraction (vdW), Pauli repulsion, and electrostatic forces.[1,20−23] Hence, the atomic models should therefore include at least these three interactions. An accurate description of the electrostatic contribution is especially important, as these can range from very weak to very strong and can be long-ranged. Since most classical force fields incorporate these interactions (in one form or another), these have been used to simulate self-assembly of molecules.[9,17−19,24−26] Additionally, methods for incorporating molecule−substrate interactions have been developed.[27−29] However, the ability to predict which crystals are stable and which are metastable has received little attention.

Here, we present an experimental and theoretical investigation of the self-assembly of molecules with different functional groups (carboxylic acids, nitrile groups, pyridine groups) on weakly interacting surfaces. This results in systems

Received: October 9, 2015
Revised: December 7, 2015
Published: December 10, 2015

DOI: 10.1021/acs.jpcc.5b09889
J. Phys. Chem. C 2016, 120, 318−323

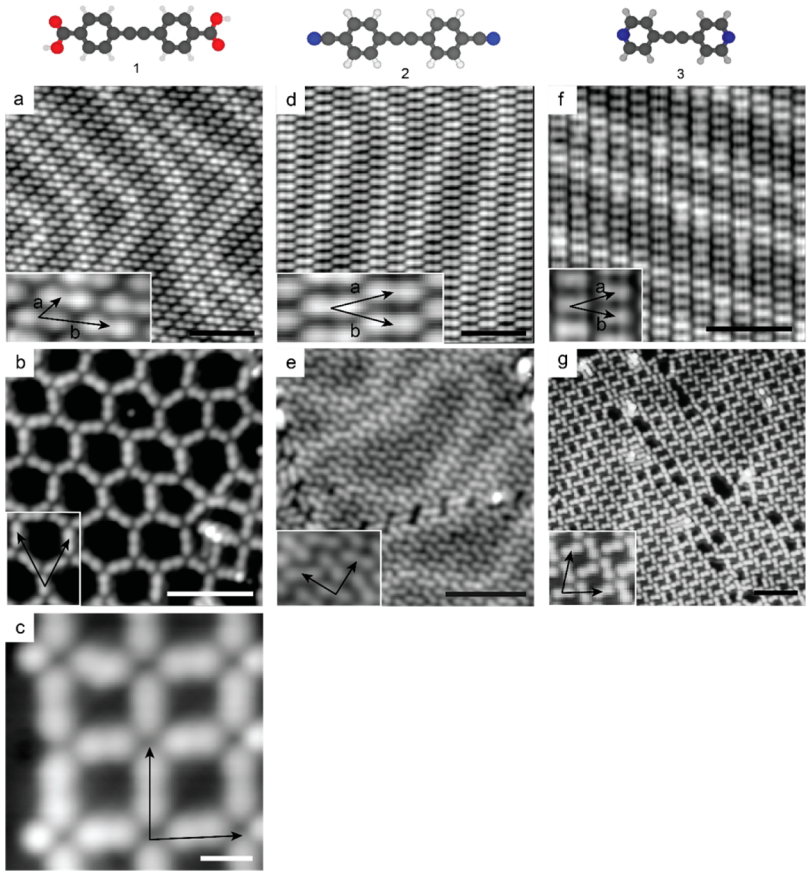

Figure 1. STM overview of self-assembled structures on Au(111). (a–c) Structures of **1**–**3**, respectively. C, N, O, and H atoms are indicated in black, blue, red, and white, respectively. (d–f) Close-packed crystals of structures of **1**–**3**, respectively. The insets shows the unit cells. (g–j) Crystals with different geometries as observed for **1** (g,j), **2** (h), and **3** (i). All images are recorded on a Au(111) surface with tunneling parameters of 0.05–0.1 V/5–10 pA. Scale bars in d–i: 5 nm, in j: 1 nm.

with strong, intermediate, and weak electrostatic interactions between molecules, respectively. We developed an atomistic model that accurately describes the forces between molecules based solely on the chemical structure of the molecules. Each atom is assigned a fractional charge, calculated from DFT, and lone pairs are explicitly taken into account. This, together with the vdW and Pauli interactions, is used as input for Monte Carlo (MC) simulations. Both stable and metastable phases are identified. In all cases, the experimentally observed crystal structures are reproduced with a sub-Ångström precision in the lattice parameters.

RESULTS AND DISCUSSION

The magnitude of the electrostatic interactions is varied by introducing different functional groups (carboxylic acid, nitrile, and pyridine) to otherwise similar molecules. The structure of the molecules (bis(*para*-benzoicacid)-acetylene, **1**, bis(*para*-cyanobenzene)-acetylene, **2**, and bis(*para*-pyridine)-acetylene, **3**) is given in Figure 1a–c, respectively. The molecules were synthesized according to literature procedures.[30−32] For details, see the Supporting Information. Molecules **1**–**3** were evaporated onto a Au(111) crystal cleaned by several sputter/anneal cycles held at room temperature from a stainless-steel crucible in an e-beam evaporator. In all cases only one type of molecule was evaporated, and the coverage was below one monolayer. After evaporation the crystal was inserted into a scanning tunneling microscope (STM) (Omicron GmbH) operating at T = 4.5 K located in the same vacuum system. The STM scanner was calibrated using a graphene on Ir(111) sample resulting in a systematic error of approximately 2%.[33]

All molecules formed at least two different structures on the Au(111) surface, an overview of which is shown in Figure 1. All three types of molecules appear as dumbbells in the STM images. Given the cooling rate of >10 K min^{-1}, it is very likely that some of these structures are metastable.[14] For all three molecules a close-packed crystal is observed (Figure 1d–f). All molecules also form self-assembled layers with a lower density (Figure 1g–j). Note that these structures are very different for the different molecules. For **1**, patches with honeycomb (Figure 1g) and square (Figure 1j) geometries are observed, whereas for **2** a "fishbone" like structure (Figure 1e) is found. **3** formed multiple lower density structures that contain a significant number of defects, one of which is shown in Figure 1i. In the following, this chiral structure is referred to as the "windmill" structure. Both stereoisomers are observed in equal amounts. As clearly seen in Figures 1d–f, the herringbone reconstruction of the Au(111) surface is visible underneath all crystals. This implies that the interaction between the molecules and the surface is weak, in line with previous experiments on π-conjugated molecules on Au(111).[34,35]

We now turn our attention to simulations of the self-assembled layers. In the absence of chemical bonding, the geometric structure of a molecule will to first order not change due to self-assembly. Hence, to model self-organization it should be sufficient to take into account only intermolecular

DOI: 10.1021/acs.jpcc.5b09889
J. Phys. Chem. C 2016, 120, 318−323

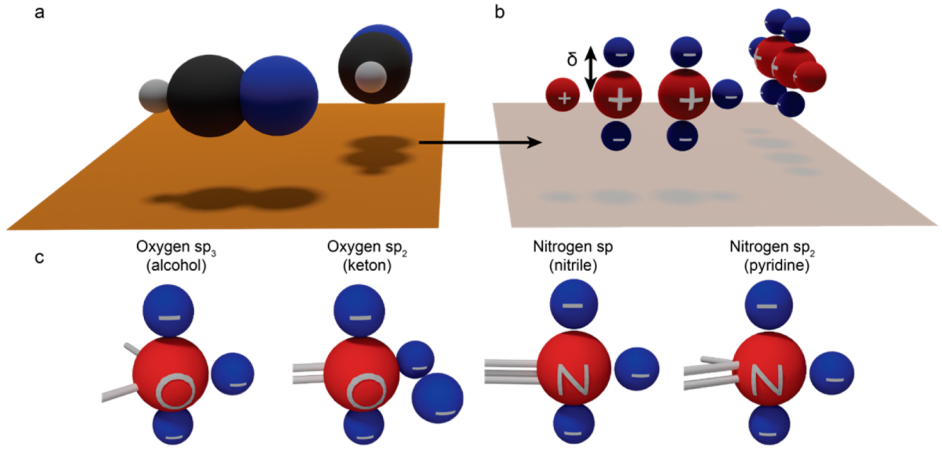

Figure 2. Atomic model to interpret molecular interactions. (a) Two HCN molecules above a weakly interacting surface. (b) Representation of the point charges in two HCN molecules comprising the electrostatic interaction. (c) Positions of the lone-pair electrons on oxygen and nitrogen atoms as used in the model.

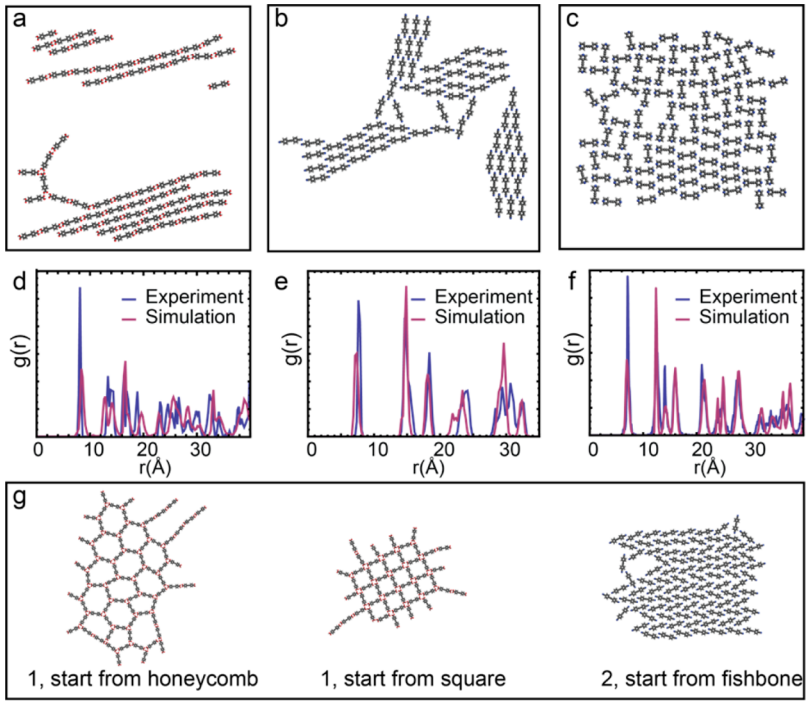

Figure 3. MC simulations of all molecules showing most stable structures. (a) Snapshot of the simulation of **1** after 4×10^6 MC cycles at $T = 500$ K in a 150 Å × 150 Å showing self-assembly. (b) Same as (a), but for **2** and after 2.5×10^6 MC cycles at $T = 275$ K. (c) Same as (a) but for **3** and after 10^6 MC cycles at $T = 150$ K. (d–f) Radial distribution functions extracted from experimental (blue) and simulation (isotension–isothermal ensemble, red) data for close-packed crystals of **1**–**3**, respectively. (g) From left to right: snapshots of simulations starting with experimentally observed honeycomb and square crystals of **1** (after 3×10^6 and 3×10^5 MC cycles, $T = 300$ K, and $T = 250$ K) and the "fishbone" crystal of **2** (after 3×10^5 MC simulations, $T = 250$ K).

interactions; i.e., we treat the molecule as a rigid body. To investigate the stability of the observed structures we propose an atomistic model that includes only vdW, Pauli, and electrostatic forces between atoms. The vdW and Pauli are modeled using parametrized pair potential function from the AMBER force field.[36] As a starting point to model the electrostatic forces between molecules, we use the model by Hunter and Sanders.[37] This model accurately describes the packing of aromatic molecules in 3D crystals. The model is illustrated in Figure 2a/b. Each atom that contributes to the π-framework is represented by three point charges (Figure 2b): a positive charge ($+1e^-$ for C, $+1.5e^-$ for N, $+2e^-$ for O) at the location of the nucleus and negative point charges ($-0.5e^-$, $-0.75e^-$, and $-1e^-$) located a distance $\delta = 0.47$ Å above and below the nucleus (Figure 2b). The value of δ is chosen such that the model reproduces the experimental value of the quadrupole moment of benzene.[38] We amend the original model by including the H atoms as single-point charges at their atomic positions (Figure 2b). In addition, lone pairs of electrons are explicitly taken into account as additional negative point charges (Figure 2b). The number and position of lone pairs around an atom are determined by its hybridization. In Figure 2c the lone pair configurations for oxygen and nitrogen used in this paper are illustrated. All lone pairs are located a

DOI: 10.1021/acs.jpcc.5b09889
J. Phys. Chem. C 2016, 120, 318–323

distance Δ_L = 0.47 Å from the positive charge. A sp^3 oxygen has one lone pair above and one lone pair below the plane. This can be modeled by including a single lone pair in the plane. The sp^2 oxygen has two lone pairs in the plane, separated by 120°. Nitrogen in a sp hybridization has one lone pair in line with the bonding direction. Finally, a sp^2 nitrogen has one lone pair in the plane directly opposite its two bonding partners. The robustness of the model with respect to variations in Δ_L is discussed in the Supporting Information.

In (nearly) all molecules, the electrons are inhomogeneously distributed over space leading to charge polarization. This charge polarization is incorporated by assigning a fractional charge to each atom. The magnitude of these partial charges is obtained by partitioning the total electron density, obtained from DFT, using the Voronoi deformation density (VDD) as implemented in the ADF package.[39,40] The magnitude of the negative point charges is determined by dividing the total negative charge of the atom ($-1e^-$ for C, $-1.5e^-$ for N, $-2e^-$ for O, corrected by the VDD charges) by the number of negative point charges surrounding it. For example, the N atom in Figure 2b (VDD: $-0.17e^-$) is modeled by one positive charge of $+1.5e^-$ and three identical negative point charges of $(-1.5-0.17e^-)/3 = -0.443e^-$. In the current implementation of the model, molecule−substrate interactions are not taken into account. Finally, the self-assembly is studied using two-dimensional Monte Carlo simulations in the canonical ensemble (details in the Supporting Information).

Snapshots of the simulation of **1**−**3** after MC runs of 4×10^6, 2.5×10^6, and 2.75×10^6 cycles are shown in Figure 3a−c, respectively. At the start of the simulations, the molecules were placed randomly in a 150 × 150 Å box, and the temperatures were fixed at T = 500, 275, and 300 K, respectively. For all molecules, patches of close-packed crystals are observed. Interestingly, for **3** also the lower density windmill structure is observed in the simulations.

To facilitate a comparison between experiment and theory, we determined the radial distribution function, $g(r)$, as well as the lattice parameters from the STM images and MC simulations. The crystals observed in the NVT simulations are rather small, making it difficult to extract meaningful parameters from these simulations. Larger crystals were obtained by using the crystals found in the NVT simulations as input for isotension−isothermal ensemble MC simulations (details in Supporting Information). The radial distribution functions are given in Figure 3d−f. In all cases the peaks overlap, indicating a good agreement. Even in the case of 2,3-naphthalocyanine (**4**) on Au(111),[23] where the electrostatic contribution to the intermolecular interaction is virtually zero, our model correctly reproduces the experimentally observed crystal structure (Figure 4). This is further corroborated by the fact that lattice parameters agree to within 0.5 Å and 2° (see Table 1). Hence, our model is able to correctly reproduce the structure of a self-assembled molecular layer for various intermolecular interaction strengths. In all cases our simulations somewhat overestimate (0.1−0.5 Å) the lattice parameters. This may be due to the choice of force field parameters as well as the omission of intramolecular relaxations.

The outcome of the simulations is robust with respect to variations in δ. In addition, we found the influence of a conductive surface, modeled by including image charges, to be negligible. However, the inclusion of lone pairs in our model is critical to correctly reproduce experimental observations. These points are further discussed in the Supporting Information.

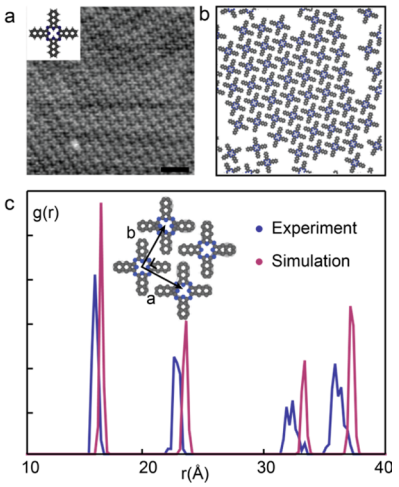

Figure 4. Self-assembly of 2,3-naphthalocyanine. (a) STM image of close-packed crystal of **4** taken at room temperature (V = −1.47 V, I = 40 pA). Scale bar: 5 nm. Data courtesy of M. Stöhr. The inset shows the chemical structure of **4**. Carbon, hydrogen, and N atoms are indicated in gray, white, and blue, respectively. (b) Self-assembly of 64 molecules after a MC run of 4.5×10^5 cycles at T = 100 K. (c) $g(r)$ extracted from the STM images (blue) and MC simulations (purple). The inset shows the unit cell of the molecular crystal.

Table 1. Lattice Parameters of Close-Packed Crystals of 1−4[a]

molecule	extracted from	lattice parameters		
		a (Å)	b (Å)	α (deg)
1	experiments	8.1	16.3	51
1	simulations	8.4	16.5	50
2	experiments	14.6	14.6	30
2	simulations	14.9	14.8	29
3	experiments	12.3	12.3	32
3	simulations	12.4	12.4	34
4	experiments	16.1	16.1	90
4	simulations	16.6	16.6	90

[a]Standard deviation for all distances and angles: 0.2 Å and 1°, respectively. The uncertainties only reflect the statistical error. The systematic error resulting from an imperfect calibration of the STM scanner is approximately 2%.

It is well-known that not all stable phases form spontaneously in typical MC simulations. Hence, to investigate the stability of the other experimentally observed crystals for **1** and **2**, we performed simulations in the canonical ensemble where we start with the experimentally observed crystals. If the simulated crystals quickly transform into another crystal or melt into a gas or liquid, then according to the model they are unstable. If they do not melt, they are either metastable or stable. Figure 3g shows snapshots of these simulations for the honeycomb and square crystal structures of **1** and the fishbone phase of **2** (after 3×10^6, 3×10^5, and 3×10^5 cycles, respectively). Simulations were performed using T = 300, 250, and 250 K, respectively. In all cases, the crystals are still intact, indicating that they are at least metastable.

To determine which structures were fully stable and which were only metastable at T = 0 K, we determined the T = 0 K phase diagram using common tangent constructions. In a common tangent construction, the Helmholtz free energy per volume is plotted as a function of the density. In this

DOI: 10.1021/acs.jpcc.5b09889
J. Phys. Chem. C 2016, 120, 318−323

representation, phase coexistence corresponds to a pair of densities for which the tangent lines to this curve have both the same slope and the same intercept, corresponding to equal pressure and chemical potential. Moreover, the stable phase at any given density corresponds to the phase (or coexistence of phases) with the lowest Helmholtz free energy per volume at the density in question. At zero temperature the Helmholtz free energy is simply equal to the potential energy, i.e., $F = U$. Hence, in Figure 5(a–c) we plot the energy per volume of the

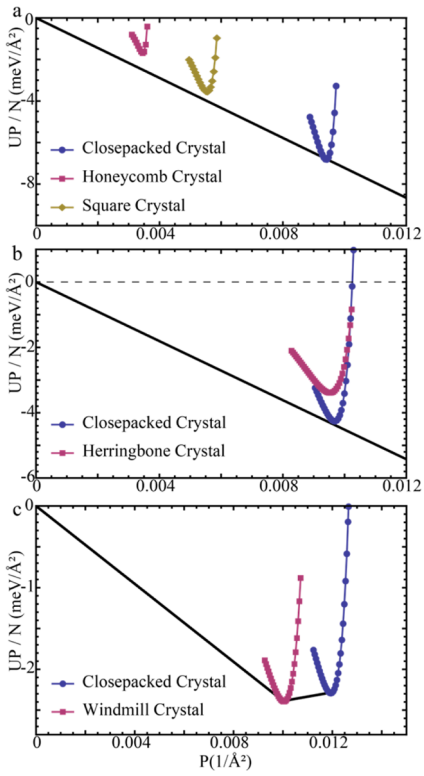

Figure 5. Common tangent constructions for **1**–**3** at $T = 0$ K. (a) For **1**, the common tangent connects the close-packed crystal with the gas phase. The honeycomb and square phase are located above the line, indicating that they are metastable. (b) For **2**, the "fishbone" structure lies above the common tangent line. (c) For **3**, both crystal structures are connected via the common tangent line and are therefore stable.

crystal phases as a function of the density for molecules **1**–**3**, respectively. We also include a gas phase in these plots. At $T = 0$ K, the gas phase is expected to have a very low density, and the molecules do not interact. Hence, the free energy of the gas phase is $F_{gas} = U_{gas} \approx 0$ meV. Both the honeycomb and square structures of **1** are clearly above the common tangent line (Figure 5a). Hence, at $T = 0$ K the two low density structures of **1** are metastable in our model, and the high density phase is stable. For **2**, the "fishbone" structure is higher in energy than the close-packed structure. It is above the common tangent line, indicating it is also metastable. In contrast, for **3** both the "windmill" crystal and the close-packed crystal are fully stable at $T = 0$ K. This explains why both phases are observed in the canonical NVT simulations: at the density where the NVT simulations shown in Figure 4c were performed, there is a coexistence of both phases.

CONCLUSIONS

In summary, we have investigated the self-assembly of three molecules with a similar backbone but with different functional groups on a weakly interacting surface. The intermolecular electrostatic interactions span nearly the entire energy range. A variety of crystal structures are observed. In addition, we developed a simple model that can be used to study the self-assembly of molecules on a weakly interacting surface. The model includes vdW, Pauli, and electrostatic interactions. The model allows us to establish which self-assembled phases are stable and which ones are metastable. We hope that the availability of a predictive model will help to speed up the research of scientists aiming to synthesize and study self-assembled molecular layers with a particular geometry. We believe that it is possible to expand the applicability of the model by including molecule–substrate interactions. For example it should be straightforward to expand the model described here to also include ionic surfaces. An alternative approach is to use potential energy grid files.[27,28]

ASSOCIATED CONTENT

Supporting Information

The Supporting Information is available free of charge on the ACS Publications website at DOI: 10.1021/acs.jpcc.5b09889.

Details of the synthesis of **1**–**3** and MC simulations. A discussion on the robustness of the model, adsorption of **2** on Ag(111). Performance of the model in the case of very weak electrostatic interactions (PDF)

AUTHOR INFORMATION

Corresponding Authors

*E-mail: l.c.filion@uu.nl.
*E-mail: i.swart@uu.nl.

Author Contributions

†These authors contributed equally.

Notes

The authors declare no competing financial interest.

ACKNOWLEDGMENTS

We are grateful to Meike Stöhr for providing the data on 2,3-naphthalocyanine. We acknowledge financial support from the Dutch Sector Plan Physics and Chemistry and The Netherlands Organization for Scientific Research (NWO-VENI grants No. 722.011.007, 680.47.432, and NWO-ECHO-STIP Grant No. 717.013.003).

REFERENCES

(1) Bartels, L. Tailoring Molecular Layers at Metal Surfaces. *Nat. Chem.* **2010**, *2*, 87–95.
(2) Blunt, M. O.; Russell, J. C.; Champness, N. R.; Beton, P. H. Templating Molecular Adsorption Using a Covalent Organic Framework. *Chem. Commun.* **2010**, *46*, 7157–7159.
(3) Yamamoto, Y.; Nishihara, H.; Aramaki, K. Self-Assembled Layers of Alkanethiols on Copper for Protection Against Corrosion. *J. Electrochem. Soc.* **1993**, *140* (2), 436.
(4) Bohrer, F. I.; Colesniuc, C. N.; Park, J.; Ruidiaz, M. E.; Schuller, I. K.; Kummel, A. C.; Trogler, W. C. Comparative Gas Sensing in Cobalt, Nickel, Copper, Zinc, and Metal-Free Phthalocyanine Chemiresistors. *J. Am. Chem. Soc.* **2009**, *131*, 478–485.
(5) Browne, W. R.; Feringa, B. L. Making Molecular Machines Work. *Nat. Nanotechnol.* **2006**, *1*, 25–35.

DOI: 10.1021/acs.jpcc.5b09889
J. Phys. Chem. C 2016, 120, 318–323

(6) Joachim, C.; Gimzewski, J. K.; Aviram, A. Electronics Using Hybrid-Molecular and Mono-Molecular Devices. *Nature* **2000**, *408*, 541−548.
(7) Barth, J. V.; Costantini, G.; Kern, K. Engineering Atomic and Molecular Nanostructures at Surfaces. *Nature* **2005**, *437*, 671−679.
(8) Pham, T. A.; Song, F.; Nguyen, M.-T.; Stöhr, M. Self-Assembly of Pyrene Derivatives on Au(111): Substituent Effects on Intermolecular Interactions. *Chem. Commun.* **2014**, *50*, 4−7.
(9) Adisoejoso, J.; Tahara, K.; Lei, S.; Szabelski, P.; Rzysko, W.; Inukai, K.; Blunt, M. O.; Tobe, Y.; De Feyter, S. One Building Block, Two Different Nanoporous Self-Assembled Monolayers: A Combined STM and Monte Carlo Study. *ACS Nano* **2012**, *6*, 897−903.
(10) Korevaar, P. A.; George, S. J.; Markvoort, A. J.; Smulders, M. M. J.; Hilbers, P. A. J.; Schenning, A. P. H. J.; De Greef, T. F. A.; Meijer, E. W. Pathway Complexity in Supramolecular Polymerization. *Nature* **2012**, *481*, 492−496.
(11) Korevaar, P. A.; Grenier, C.; Markvoort, A. J.; Schenning, A. P. H. J.; de Greef, T. F. A.; Meijer, E. W. Model-Driven Optimization of Multicomponent Self-Assembly Processes. *Proc. Natl. Acad. Sci. U. S. A.* **2013**, *110*, 17205−17210.
(12) Cui, H.; Chen, Z.; Zhong, S.; Wooley, K. L.; Pochan, D. J. Block Copolymer Assembly via Kinetic Control. *Science* **2007**, *317*, 647−650.
(13) Müller, M.; Sun, D.-W. Directing the Self-Assembly of Block Copolymers into a Metastable Complex Network Phase via a Deep and Rapid Quench. *Phys. Rev. Lett.* **2013**, *111*, 267801.
(14) Shang, J.; Wang, Y.; Chen, M.; Dai, J.; Zhou, X.; Kuttner, J.; Hilt, G.; Shao, X.; Gottfried, J. M.; Wu, K. Assembling Molecular Sierpiński Triangle Fractals. *Nat. Chem.* **2015**, *7*, 389−393.
(15) Ciesielski, A.; Szabelski, P. J.; Rżysko, W.; Cadeddu, A.; Cook, T. R.; Stang, P. J.; Samorì, P. Concentration-Dependent Supramolecular Engineering of Hydrogen-Bonded Nanostructures at Surfaces: Predicting Self-Assembly in 2D. *J. Am. Chem. Soc.* **2013**, *135*, 6942−6950.
(16) Nieckarz, D.; Szabelski, P. Understanding Pattern Formation in 2D Metal−Organic Coordination Systems on Solid Surfaces. *J. Phys. Chem. C* **2013**, *117*, 11229−11241.
(17) Vijayaraghavan, S.; Ecija, D.; Auwärter, W.; Joshi, S.; Seufert, K.; Drach, M.; Nieckarz, D.; Szabelski, P.; Aurisicchio, C.; Bonifazi, D.; et al. Supramolecular Assembly of Interfacial Nanoporous Networks with Simultaneous Expression of Metal-Organic and Organic-Bonding Motifs. *Chem. - Eur. J.* **2013**, *19*, 14143−14150.
(18) Palma, C. A.; Samorì, P.; Cecchini, M. Atomistic Simulations of 2D Bicomponent Self-Assembly: From Molecular Recognition to Self-Healing. *J. Am. Chem. Soc.* **2010**, *132*, 17880−17885.
(19) Martsinovich, N.; Troisi, A. Modeling the Self-Assembly of Benzenedicarboxylic Acids Using Monte Carlo and Molecular Dynamics Simulations. *J. Phys. Chem. C* **2010**, *114*, 4376−4388.
(20) Slater (née Phillips), A. G.; Beton, P. H.; Champness, N. R. Two-Dimensional Supramolecular Chemistry on Surfaces. *Chem. Sci.* **2011**, *2*, 1440−1448.
(21) Yokoyama, T.; Yokoyama, S.; Kamikado, T.; Okuno, Y.; Mashiko, S. Selective Assembly on a Surface of Supramolecular Aggregates with Controlled Size and Shape. *Nature* **2001**, *413*, 619−621.
(22) Rabe, J. P.; Buchholz, S. Commensurability and Mobility in Two-Dimensional Molecular Patterns on Graphite. *Science* **1991**, *253*, 424−427.
(23) Pham, T. A.; Song, F.; Stöhr, M. Supramolecular Self-Assembly of Metal-Free Naphthalocyanine on Au(111). *Phys. Chem. Chem. Phys.* **2014**, *16*, 8881−8885.
(24) Kasperski, A.; Szabelski, P. Two-Dimensional Molecular Sieves: Structure Design by Computer Simulations. *Adsorption* **2013**, *19*, 283−289.
(25) Clair, S.; Pons, S.; Seitsonen, A. P.; Brune, H.; Kern, K.; Barth, J. V. STM Study of Terephthalic Acid Self-Assembly on Au(111): Hydrogen-Bonded Sheets on an Inhomogeneous Substrate. *J. Phys. Chem. B* **2004**, *108*, 14585−14590.
(26) Ciesielski, A.; Stefankiewicz, A. R.; Hanke, F.; Persson, M.; Lehn, J. M.; Samorì, P. Rigid Dimers Formed through Strong Interdigitated H-Bonds Yield Compact 1D Supramolecular Helical Polymers. *Small* **2011**, *7*, 342−350.
(27) Mannsfeld, S.; Fritz, T. Analysis of the Substrate Influence on the Ordering of Epitaxial Molecular Layers: The Special Case of Point-on-Line Coincidence. *Phys. Rev. B: Condens. Matter Mater. Phys.* **2004**, *69*, 1−9.
(28) Mannsfeld, S. C. B.; Fritz, T. Understanding Organic-Inorganic Heteroepitaxial Growth of Molecules on Crystalline Substrates: Experiment and Theory. *Phys. Rev. B: Condens. Matter Mater. Phys.* **2005**, *71*, 1−10.
(29) Roussel, T. J.; Barrena, E.; Ocal, C.; Faraudo, J. Predicting Supramolecular Self-Assembly on Reconstructed Metal Surfaces. *Nanoscale* **2014**, *6*, 7991−8001.
(30) Berger, O.; Kaniti, A.; van Ba, C. T.; Vial, H.; Ward, S. A.; Biagini, G. A.; Bray, P. G.; O'Neill, P. M. Synthesis and Antimalarial Activities of a Diverse Set of Triazole-Containing Furamidine Analogues. *ChemMedChem* **2011**, *6*, 2094−2108.
(31) Fasina, T. M.; Collings, J. C.; Burke, J. M.; Batsanov, A. S.; Ward, R. M.; Albesa-Jové, D.; Porrès, L.; Beeby, A.; Howard, J. A. K.; Scott, A. J.; et al. Synthesis, Optical Properties, Crystal Structures and Phase Behaviour of Symmetric, Conjugated Ethynylarene-Based Rigid Rods with Terminal Carboxylate Groups. *J. Mater. Chem.* **2005**, *15*, 690−697.
(32) Coe, B. J.; Harries, J. L.; Harris, J. A.; Brunschwig, B. S.; Coles, S. J.; Light, M. E.; Hursthouse, M. B. Syntheses, Spectroscopic and Molecular Quadratic Nonlinear Optical Properties of Dipolar ruthenium(II) Complexes of the Ligand 1,2-Phenylenebis-(dimethylarsine). *Dalton Trans.* **2004**, 2935−2942.
(33) Boneschanscher, M. P.; Hämäläinen, S. K.; Liljeroth, P.; Swart, I. Sample Corrugation Affects the Apparent Bond Lengths in Atomic Force Microscopy. *ACS Nano* **2014**, *8*, 3006−3014.
(34) Soe, W. H.; Manzano, C.; De Sarkar, A.; Chandrasekhar, N.; Joachim, C. Direct Observation of Molecular Orbitals of Pentacene Physisorbed on Au(111) by Scanning Tunneling Microscope. *Phys. Rev. Lett.* **2009**, *102*, 176102.
(35) Van der Lit, J.; Boneschanscher, M. P.; Vanmaekelbergh, D.; Ijäs, M.; Uppstu, A.; Ervasti, M.; Harju, A.; Liljeroth, P.; Swart, I. Suppression of Electron-Vibron Coupling in Graphene Nanoribbons Contacted via a Single Atom. *Nat. Commun.* **2013**, *4*, 2023.
(36) Cornell, W. D.; Cieplak, P.; Bayly, C. I.; Gould, I. R.; Merz, K. M.; Ferguson, D. M.; Spellmeyer, D. C.; Fox, T.; Caldwell, J. W.; Kollman, P. A. A Second Generation Force Field for the Simulation of Proteins, Nucleic Acids, and Organic Molecules. *J. Am. Chem. Soc.* **1995**, *117*, 5179−5197.
(37) Hunter, C. A.; Sanders, J. K. M. The Nature of π-π Interactions. *J. Am. Chem. Soc.* **1990**, *112*, 5525−5534.
(38) Price, S. L.; Stone, A. J. The Electrostatic Interactions in van Der Waals Complexes Involving Aromatic Molecules. *J. Chem. Phys.* **1987**, *86*, 2859.
(39) Fonseca Guerra, C.; Handgraaf, J.-W.; Baerends, E. J.; Bickelhaupt, F. M. Voronoi Deformation Density (VDD) Charges: Assessment of the Mulliken, Bader, Hirshfeld, Weinhold, and VDD Methods for Charge Analysis. *J. Comput. Chem.* **2004**, *25*, 189−210.
(40) te Velde, G.; Bickelhaupt, F. M.; Baerends, E. J.; Fonseca Guerra, C.; van Gisbergen, S. J. A.; Snijders, J. G.; Ziegler, T. Chemistry with ADF. *J. Comput. Chem.* **2001**, *22*, 931−967.

DOI: 10.1021/acs.jpcc.5b09889
J. Phys. Chem. C 2016, 120, 318−323